Title
Growth Kinetics of Intermetallic Compounds Between Sn and Fe Liquid–Solid Reaction Couples

Journal
Journal of Electronic Packaging, 138(4)

ISSN
1043-7398

Authors
Hsu, Shou-Jen
Lee, Chin C

Publication Date
2016-12-01

DOI
10.1115/1.4034842

Growth Kinetics of Intermetallic Compounds between Sn and Fe Liquid-Solid Reaction Couples

Shou-Jen Hsu and Chin C. Lee
Electrical Engineering and Computer Science
Materials and Manufacturing Technology
University of California
Irvine, CA 92697-2660

Abstract

Growth behavior of the intermetallic compound (IMC), $FeSn_2$, was investigated in the liquid Sn/solid Fe reaction couple over the annealing temperatures from 250°C to 400°C. Low carbon steel AISI 1018 was chosen to make Fe samples. The morphology and thickness of the IMC formed between Sn and Fe were examined using scanning electron microscopy (SEM). In addition, energy-dispersive X-ray spectroscopy (EDX) and X-ray diffraction (XRD) were used to confirm that the IMC is $FeSn_2$. The growth kinetics of $FeSn_2$ was modeled by parabolic law and empirical power law. Based on the models, the growth constants, activation energy and time exponents were established at different annealing temperatures. It was found that the time exponent values obtained by fitting with empirical power law deviate from 0.5, meaning that volume (bulk) diffusion is not the only rate-controlling process in the liquid Sn/solid Fe reaction couple. Also, a variation in the time exponent values is indicative that the growth behavior is correlated with grain size growth and irregular grain morphology at different annealing stages. The results of this research show that AISI 1018 steel can readily react with Sn to form IMC on the interface. This is an essential requirement of soldering action using Sn-rich solders.

Keywords: solder; intermetallic compound; tin; low carbon steel

1. Introduction

Ferrous metals have had various applications in automotive and electronic industries. Ultra low carbon, low carbon, and micro-alloyed steels have been widely used as auto body material [1-3]. Invar (Fe-36Ni) is known for its uniquely low coefficient of thermal expansion (CTE) around 0.8 to 1.6 ppm/°C (measured between 30-100°C). It has been utilized in manufacturing precision instruments where high dimensional stability is required. Alloy 42 (Fe-42Ni) and Kovar (Fe-29Ni-17Co) are controlled expansion alloys with CTE of 4.0 to 4.7 ppm/°C (measured at 30-300°C) and 5.1 to 5.5 ppm/°C (measured at 30-

450°C), respectively [4-6]. In electronics, these alloys have been used to make lead-frames of plastic packages and headers of transistor packages because their CTE is close to that of silicon (3 ppm/°C) and lead-sealing glass. They have also been chosen for manufacturing headers of laser diodes because their CTE matches well with that of gallium arsenide (GaAs) semiconductor (7 ppm/°C). One downside of these alloys is the relatively low thermal conductivity (10-17 W/m-K) [7]. We thus looked into ferrous metals that have higher thermal conductivity and reasonably low CTE for electronic packaging applications. After a thorough search, AISI 1018 low carbon steel was selected for this study. It has thermal conductivity of 51.9 W/m-K and CTE of 11.5 ppm/°C [8].

During the process of producing the metallic bonding between solder and metal, molten phase solder wets metal surface and reacts with metal to form an intermetallic compound (IMC) layer between solder and metal. However, the brittle nature of IMC could make it possible to be the most vulnerable point in the solder joint. Last but not least, the formation of IMC occurs not only by liquid (molten solder)-solid (metal) reaction during reflow process but by the solid-solid reaction during storage and service life. It is therefore essential to study the mechanism and kinetics of the formation of IMC at the lead-free solders/metal substrate interface. The aim of this work is to explore the growth behavior of intermetallic compound between electroplated tin (Sn) and iron (Fe) at the temperatures above the melting point of Sn (231.93°C). Although the IMC formation could be more complicated in soldering process since sometimes other metals also involve in the IMC composition, the impact from other metals is not considered in this research. In what follow, experimental design is first presented. Experimental results are reported and discussed. A brief summary is then given.

2. Experimental design

Substrates of 15 mm×13 mm×3.3 mm (width×length×thickness) were cut from AISI 1018 low carbon steel (Fe) sheet. They were ground using 800 and 1200 grit SiC-coated papers to smoothen out the surface. They were cleaned with acetone and deionized water before electroplating. Sn of 85 μm thick was electroplated over the Fe substrate in a stannous methanesulfonate bath under the condition of 43°C and pH of 1 with current density of 30 mA/cm^2. Matte Sn electroplating solution was chosen instead of bright Sn because matte is less prone to whisker formation [9]. The Sn-coated Fe substrates were then treated isothermally at 250°C, 335°C and 400°C for different durations of time in a convection furnace that had been preheated to the desired temperature. After the reactions, the Sn-coated Fe substrates were cooled in air and then mounted in epoxy resin. The samples were then cross-sectioned into halves. Microstructure observation and composition analysis were studied using scanning electron microscopy (SEM) and energy-dispersive X-ray spectroscopy (EDX). The composition of the IMC was also studied by X-ray diffraction (XRD) after etching the reacted Sn-coated Fe substrate with diluted HCl.

3. Results and discussion

3.1 Microstructural evolution of the intermetallic compound layer

Figure 1 exhibits the cross-section SEM images of the interfacial layer between Sn and Fe reacted at 250°C for 2, 12, 50, and 200 hours, respectively. It was seen that molten Sn reacted readily with Fe to form IMC, an essential requirement of soldering action. ~~This indicates that Fe is easily solderable without using flux, provided that the soldering interface is free of oxides.~~ To estimate the average thickness of the IMC layer, the region of IMC layer was first evaluated using image processing software. The average thickness was then determined by dividing the area of the IMC layer by the total length of the interface from the cross-section SEM micrographs. The average IMC thickness obtained is 5.8 μm after isothermal annealing at 250°C for 2 hours as shown in Figure 1(a). A thin layer of IMC about 1 μm was formed adjacent to Fe, which is composed of many IMC granules. IMC also grew vertically toward Sn matrix to form columnar crystals of different lengths, ranging from submicron to 5 μm. It was observed that some IMC columnar crystals detached from the continuous IMC layer and drifted into to the Sn solder bulk. This “spalling behavior” is similar to the literature data reported by Lin et al. and Teo et al [10-11]. EDX analysis confirmed the IMC composition to be $FeSn_2$, as shown in Table 1. As annealing time increased to 12 hours, it was seen that the columnar IMC crystals grew in both longitudinal and lateral direction as displayed in Figure 1(b). The average IMC thickness increased to 8.7 μm. Figure 1(c) and 1(d) shows the SEM image after annealing at 250°C for 50 and 200 hours, respectively. After prolonged annealing, the columnar IMC crystals continued ripening and started to agglomerate together, and ultimately formed a continuous IMC layer. The average IMC thicknesses after annealing at 250°C for 50 and 200 hours were estimated to be 13.3 and 20.9 μm, respectively.

Presented in Figure 2 are the cross-section SEM images of the interfacial layer between Sn and Fe reacted at 335°C for 2, 12, 50 and 100 hours. Compared to the samples annealed at 250°C, the columnar IMC crystals in the samples annealed at 355°C exhibit more rounded edges. With longer annealing time up to 50 hours, the spalling behavior became obvious. It was also observed that, when the annealing was extended to 100 hours, a large amount of the IMC spalled off and sporadically distributed in Sn matrix. Similar to the samples annealed at 250°C, the only IMC found is $FeSn_2$ as examined by EDX analysis. The chemical composition is shown in Table 1. The average IMC thicknesses of the samples annealed at 335°C for 2, 12, 50 and 100 hours are 10.3, 23.0, 44.9 and 62.2 μm, respectively.

As the annealing temperature increased to 400°C, IMC grew faster and the morphology is more irregular in comparison with the samples annealed at 335°C, as depicted in Figure 3. The average IMC thicknesses of the samples annealed at 400°C for 0.5, 2, 15 and 25 hours are 9.9, 20.5, 53.4 and 75.3 μm, respectively. XRD pattern obtained from the top surface of the etched sample reacted at 400°C for 25 hours is shown in Figure 4. Only Sn and $FeSn_2$ were identified in the XRD pattern. This is in agreement

with the results obtained from EDX analysis (Table 1) that only $FeSn_2$ was found at the interface, so were observed in the samples after annealing at 250°C and 335°C. Although FeSn is also shown as a stable IMC in the Fe-Sn binary phase diagram, FeSn IMC was not identified [12]. This result is consistent with the observations in other Sn-containing solder/ferrous metal reaction systems [13-15].

3.2 Growth kinetics of the intermetallic compound layer

The data of the average $FeSn_2$ IMC thickness with respect to annealing time for each annealing temperature are plotted in Figure 5(a). It is evident that the average IMC thickness increases as the annealing time and annealing temperature increases. Assuming that IMC formation is diffusion-controlled, the parabolic law holds.

$$d = k t^{\frac{1}{2}} \qquad (1)$$

Here, d is the average IMC thickness, t is the annealing time, k is the parabolic growth constant. This equation is derived from Fick's first law based upon the assumptions: (1) the change in concentration of diffusing components with distance within the IMC layer is linear and (2) the concentration of diffusing components at interlayer boundaries is constant [16-17]. The average $FeSn_2$ IMC thicknesses in meters are plotted as a function of the square root of the annealing time in seconds for each annealing temperature and fitted with least-squares linear regression, as displayed in Figure 6, so as to determine the values of k for each annealing temperature. The evaluated values of k are 1.96×10^{-8}, 1.01×10^{-7} and 2.56×10^{-7} $m/s^{1/2}$ at 250°C, 335°C and 400°C, respectively. The k values are subsequently analyzed to find the activation energy (Q) for the diffusion-controlled IMC growth using the Arrhenius equation,

$$k = k_0 \exp\left(\frac{-Q}{RT}\right) \qquad (2)$$

where k_0 is the pre-exponential factor, Q is the activation energy, R is the gas constant and T is the absolute temperature. Therefore, as shown in Figure 7, the activation energy obtained from the plot of ln(k) versus 1/T is 50 KJ/mol (0.52 eV). This value is smaller than those reported previously [18-20], where different annealing time, temperature and environment were conducted and diffusion couples were made with different process.

Analyzing the data shows the growth kinetics may also be modeled with an empirical power law:

$$d = k t^{n} \qquad (3)$$

Equation 3 is analogous to equation 1, except that the time exponent, n, is adopted as a variable. Figure 5(b) presents the regression curves. The values of time exponent, n, obtained by regression analysis, are 0.298, 0.466 and 0.509 at 250°C, 335°C and 400°C, respectively. The growth exponent, n, at 250°C takes a value of 0.298. The value deviates from the value (0.5) in parabolic law, indicating that the layer growth

mechanism is not a simple Fickian diffusion process whereby volume (bulk) diffusion is assumed as the predominant diffusion path. In fact, it is possible that not only volume (bulk) diffusion but other diffusion paths contribute to the rate-controlling process as well. For instance, grain boundaries, dislocations and free surfaces are high-diffusivity paths or diffusion short circuits [21] in metals. Here, grain boundary diffusion could account for this deviation from parabolic law. As can be seen in Figure 1, at early stage (annealed for 12 hours) of the annealing process, the grain sizes of the IMC near the interface close to Fe is small, suggesting that there are still enough fast paths (grain boundaries) for the interdiffusion of Sn and Fe atoms at the interface. In the course of time, the IMC grain size grows larger and the density of grain boundary is reduced. At some point the grain become large enough and connect together to form a continuous layer of IMC, as displayed in Figure 1(d), the slow path (volume diffusion) turns out to take over the major diffusion transport mechanism. This is manifested by the observation of flatten-out of the growth curve at prolonged annealing time for annealing at 250°C. Similar studies in the literature have reported that the growth exponents range from 0.25 to 0.32 for similar solid-liquid reactive diffusion couples [22-24]. On the other hand, the obtained growth exponents are close to 0.5 for the annealing experiments conducted at higher temperatures: 0.466 at 335°C and 0.509 at 400°C. This means that the growth kinetics at 335°C and 400°C is diffusion-controlled. The spalling-out of large amount of IMC occurred at higher annealing temperature explains that the growth kinetics complies with parabolic law. At higher annealing temperature, the diffusing components have higher mobility so as to the rate of formation IMC is faster. The IMC grows quickly but some of them float towards to Sn molten phase. The IMC grains do not have chance to undergo grain growth or Ostwald ripening. As shown in Figure 2(d) and Figure 3(d), the IMC does not form a continuous layer but sporadically distributes in the Sn matrix. The channels between IMC grains provide enough interdiffussion paths of reaction components. It is also worth mentioning that the irregular morphology of the IMC could cause the disparity of growth exponent values as well. The parabolic model derived from Fick's first law is based on assumptions as mentioned previously. It is assumed that the change in concentration of diffusing components with distance within the IMC layer is linear. This reminds us of the fact that this is not the situation in the real case though. The shape of IMC varies from spherical to ellipsoidal or elongated columnar. At higher annealing temperature, the IMC even disintegrates into fragments. Here, the concentration of diffusing components, Sn and Fe atoms, cannot be linear with the $FeSn_2$ IMC layer. This makes the assumption inadequate in real case.

4. Summary

The Sn-Fe liquid-solid reactive diffusion couple was experimentally studied. The diffusion couples were prepared by electroplating matte Sn on low carbon steel and then annealed in air at 250, 335 and 400°C with various annealing time. Only $FeSn_2$ was recognized as the intermetallic compound at the

interface. The $FeSn_2$ intermetallic compounds mainly grew towards Sn matrix with different geometrical shapes. Some of them spalled off the continuous intermetallic layer. It was also found that, at higher annealing temperatures and longer annealing time, the fragmented IMC was formed and scattered in the Sn matrix sporadically. The growth kinetics of the intermetallic compound was first investigated using diffusion-controlled model. The obtained activation energy for the formation of the intermetallic compound is 50 KJ/mol. Further analyses showed that the average intermetallic compound thickness better obeys the empirical power function where the time exponent of the growth is not 0.5 as described in the diffusion-controlled model. The time exponents were evaluated to be 0.298, 0.466 and 0.509 at 250°C, 335°C and 400°C, respectively. The discrepancy of the time exponents is probably attributed to the effect of grain growth and the irregular morphological microstructures of the intermetallic compound layer.

References

[1] M. M. Pour, F. Bodaghi, and M. Moshrefifar, "Surface modification of low carbon steel substrate by Al-rich clad layer applied by GTAW," *Surface & Coatings Technology*, vol. 206, pp. 217-223, Oct 25 2011.

[2] J. Hu, L.-X. Du, J.-J. Wang, and Q.-Y. Sun, "Cooling process and mechanical properties design of hot-rolled low carbon high strength microalloyed steel for automotive wheel usage," *Materials & Design*, vol. 53, pp. 332-337, Jan 2014.

[3] S. K. Paul, A. Raj, P. Biswas, G. Manikandan, and R. K. Verma, "Tensile flow behavior of ultra low carbon, low carbon and micro alloyed steel sheets for auto application under low to intermediate strain rate," *Materials & Design*, vol. 57, pp. 211-217, May 2014.

[4] http://www.edfagan.com/controlled-low-expansion-alloy-thermal-expansion-table.php

[5] D. Briand, P. Weber, and N. F. de Rooij, "Bonding properties of metals anodically bonded to glass," *Sensors and Actuators A-Physical*, vol. 114, pp. 543-549, Sep 1 2004.

[6] ASM Handbook Volume 2: Properties and Selection: Nonferrous Alloys and Special-Purpose Materials, ASM International, 1990, pp. 889–896.

[7] http://www.edfagan.com/controlled-low-expansion-alloy-physical-mechanical-properties.php

[8] ASM Handbook Volume 1: Properties and Selection: Irons, Steels, and High-Performance Alloys, ASM International, 1990, pp. 195–199.

[9] C. Jaewon, S. K. Kang, L. Jae-Ho, K. Keun-Soo, and L. Hyuck Mo, "Investigation of Sn Whisker Growth in Electroplated Sn and Sn-Ag as a Function of Plating Variables and Storage Conditions," Journal of Electronic Materials, vol. 43, pp. 259-269, Jan. 2014.

[10] Y. C. Lin and J. G. Duh, "Phase transformation of the phosphorus-rich layer in SnAgCu/Ni-P solder joints," *Scripta Materialia*, vol. 54, pp. 1661-1665, May 2006.

[11] J. W. R. Teo and Y. F. Sun, "Spalling behavior of interfacial intermetallic compounds in Pb-free solder joints subjected to temperature cycling loading," *Acta Materialia*, vol. 56, pp. 242-249, Jan 2008.

[12] C. E. T. White and H. Okamoto, Phase diagrams of indium alloys and their engineering applications: Indium Corporation of America, 1992, pp. 385–392.

[13] C. W. Hwang, K. Suganuma, J. G. Lee, and H. Mori, "Interface microstructure between Fe-42Ni alloy and pure Sn," *Journal of Materials Research*, vol. 18, pp. 1202-1210, May 2003.

[14] Y.-C. Huang, S.-W. Chen, W. Gierlotka, C.-H. Chang, and J.-C. Wu, "Dissolution and interfacial reactions of Fe in molten Sn-Cu and Sn-Pb solders," Journal of Materials Research, vol. 22, pp. 2924-2929, Oct 2007.

[15] Y.-W. Yen, H.-M. Hsiao, S.-W. Lin, P.-J. Huang, and C. Lee, "Interfacial Reactions in Sn/Fe-xNi Couples," *Journal of Electronic Materials*, vol. 41, pp. 144-152, Jan 2012.

[16] V. I. Dybkov, "Reaction Diffusion in Heterogeneous Binary Systems. 1. Growth of the Chemical Compound Layers at the Interface between Two Elementary Substances: One Compound Layer," *Journal of Materials Science*, vol. 21, pp. 3078-3084, Sep 1986.

[17] H. Liu, K. Wang, K. E. Aasmundtveit, and N. Hoivik, "Intermetallic Compound Formation Mechanisms for Cu-Sn Solid-Liquid Interdiffusion Bonding," *Journal of Electronic Materials*, vol. 41, pp. 2453-2462, Sep 2012.

[18] R. P. Frankenthal and A. W. Loginow, "Kinetics of the formation of the iron-tin alloy $FeSn_2$," *Journal of the Electrochemical Society*, vol. 107, pp. 920-923, 1960.

[19] J. A. Vanbeek, S. A. Stolk, and F. J. J. Vanloo, "Multiphase diffusion in the systems Fe-Sn and Si-Sn," *Zeitschrift Fur Metallkunde*, vol. 73, pp. 439-444, 1982.

[20] M. Hida and M. Kajihara, "Observation on Isothermal Reactive Diffusion between Solid Fe and Liquid Sn," *Materials Transactions*, vol. 53, pp. 1240-1246, Jul 2012.

[21] H. Mehrer, Diffusion in Solids: Fundamentals, Methods, Materials, Diffusion-Controlled Processes: Springer, 2007, pp. 547-548.

[22] M. Schaefer, R. A. Fournelle, and J. Liang, "Theory for intermetallic phase growth between Cu and liquid Sn-Pb solder based on grain boundary diffusion control," *Journal of Electronic Materials*, vol. 27, pp. 1167-1176, Nov 1998.

[23] J. Liang, N. Dariavach, P. Callahan, and D. Shangguan, "Metallurgy and kinetics of liquid-solid interfacial reaction during lead-free soldering," *Materials Transactions*, vol. 47, pp. 317-325, Feb 2006.

[24] H. Liu, K. Wang, K. E. Aasmundtveit, and N. Hoivik, "Intermetallic Compound Formation Mechanisms for Cu-Sn Solid-Liquid Interdiffusion Bonding," *Journal of Electronic Materials*, vol. 41, pp. 2453-2462, Sep 2012.

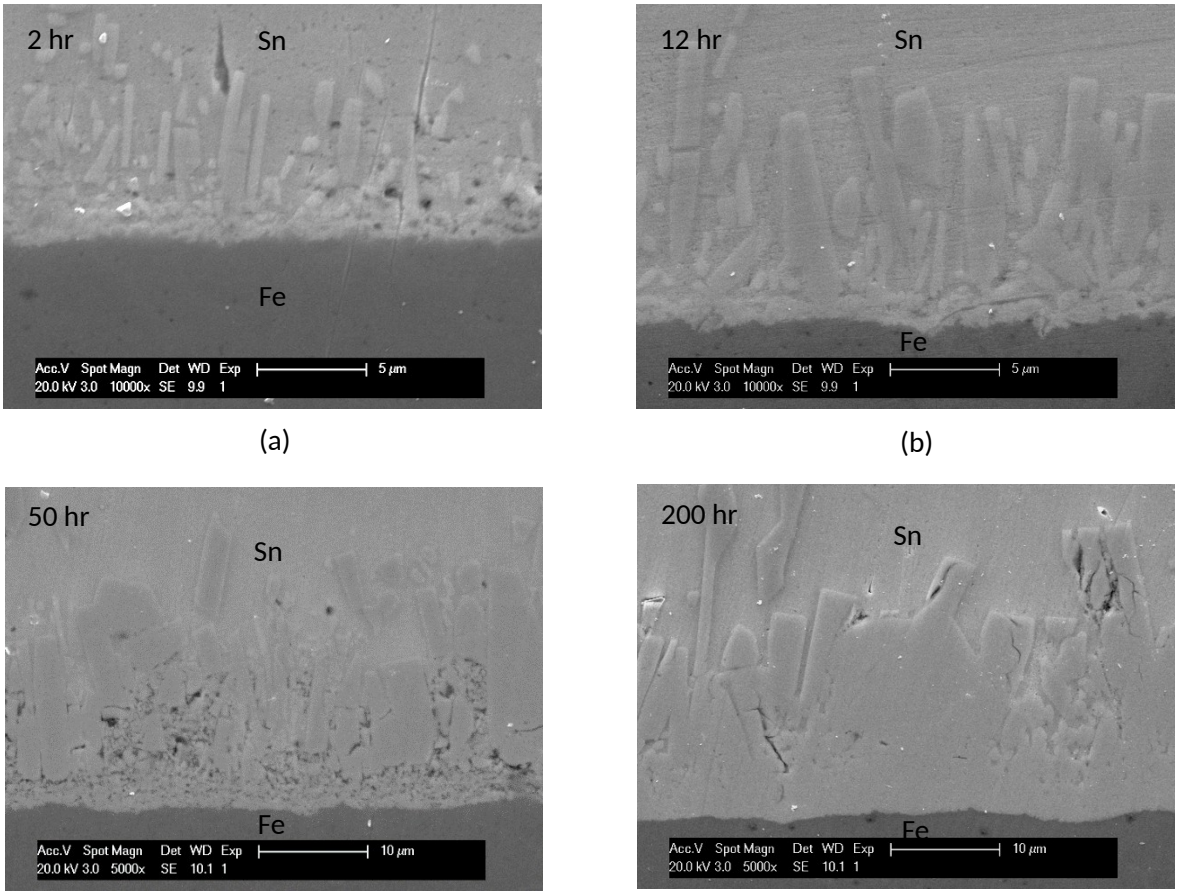

Figure 1 Cross-section SEM micrographs of the interfacial layers between Sn solder and Fe metal substrates annealed at 250°C for (a) 2 hr, (b) 12 hr, (c) 50 hr and (d) 200 hr.

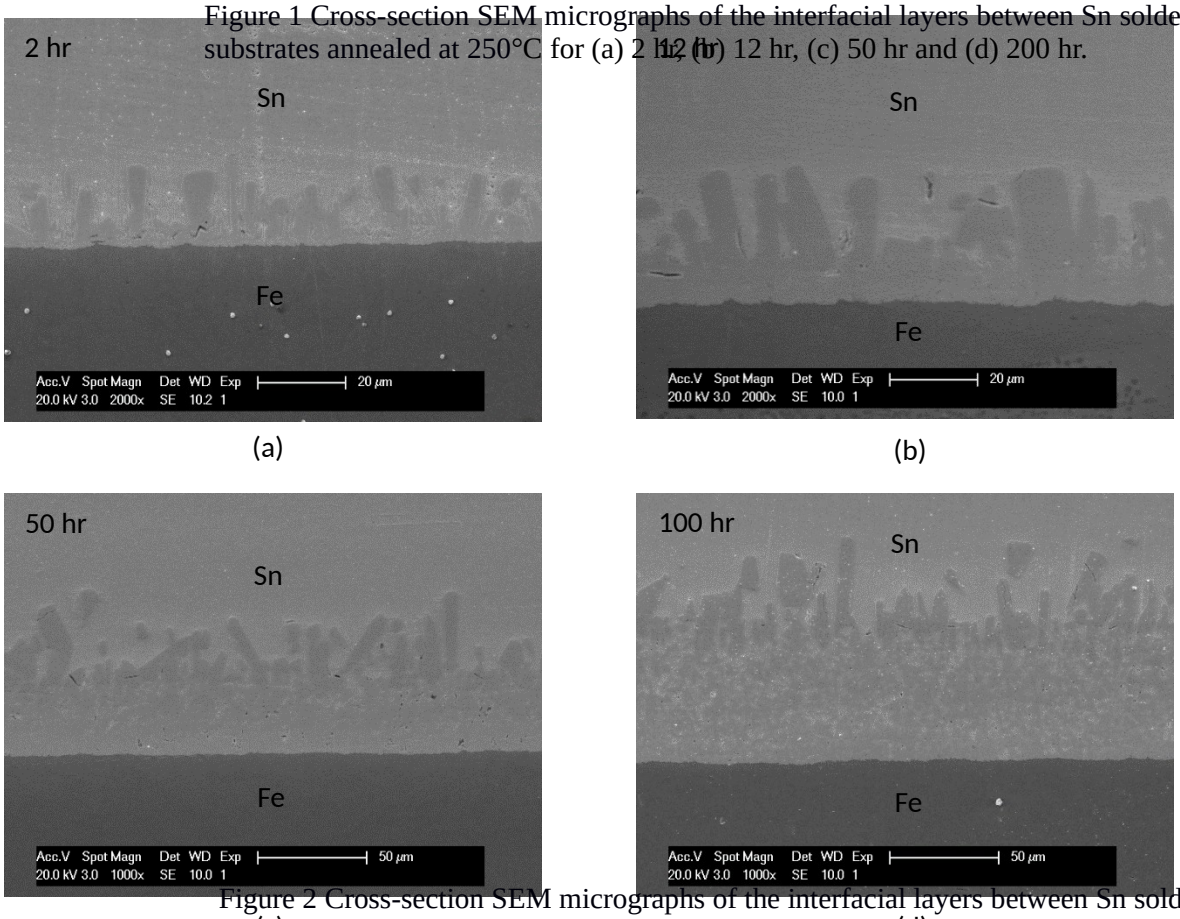

Figure 2 Cross-section SEM micrographs of the interfacial layers between Sn solder and Fe metal substrates annealed at 335°C for (a) 2 hr, (b) 12 hr, (c) 50 hr and (d) 100 hr

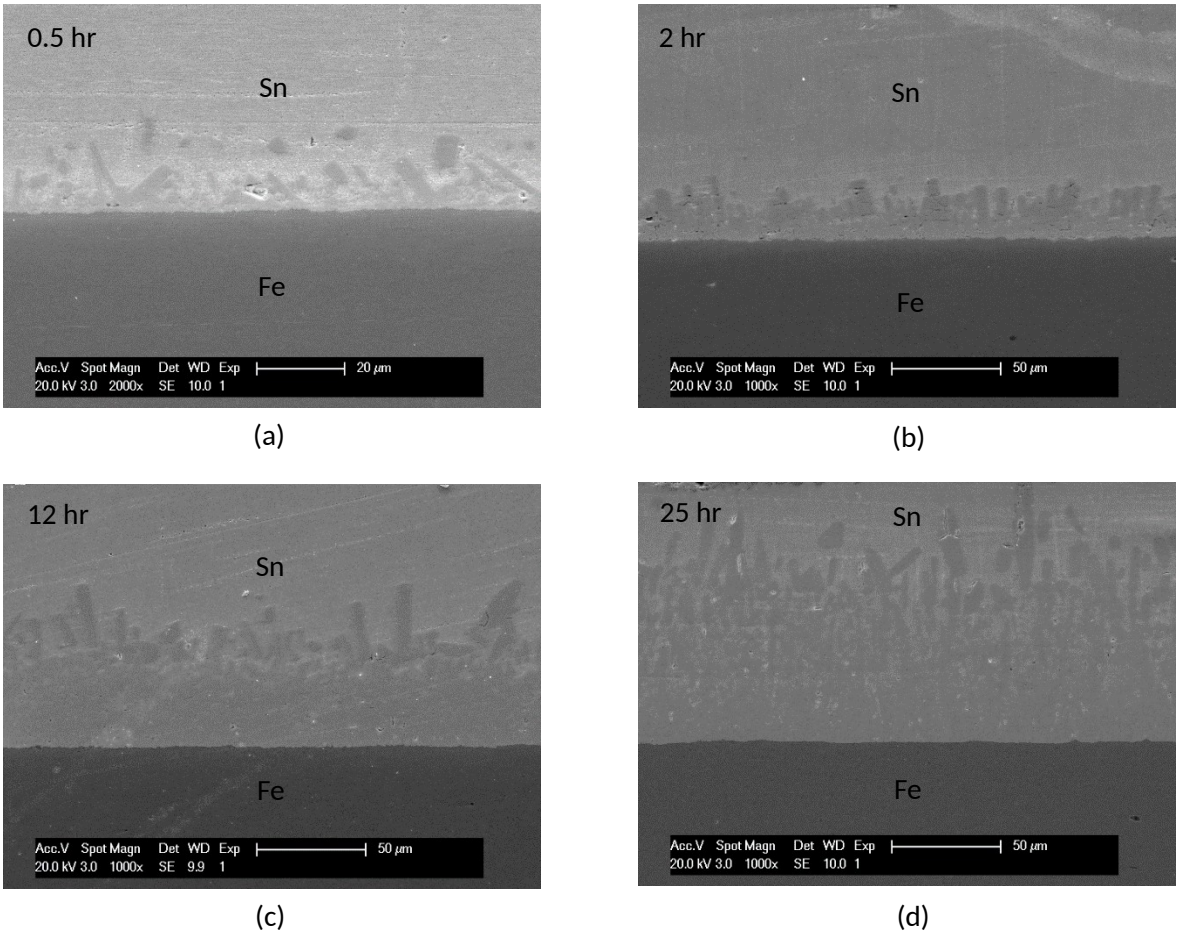

Figure 3 Cross-section SEM micrographs of the interfacial layers between Sn solder and Fe metal substrates annealed at 400°C for (a) 0.5 hr, (b) 2 hr, (c) 12 hr and (d) 25 hr.

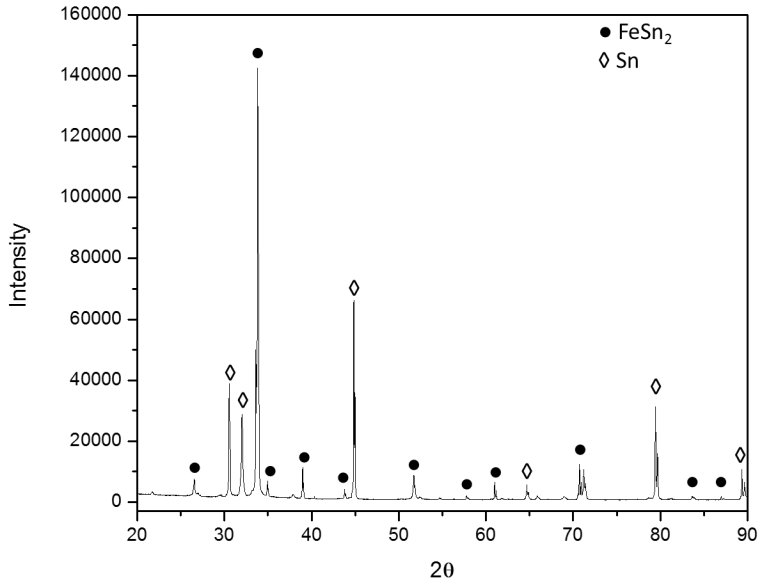

Figure 4 X-ray diffraction pattern obtained from the top surface of the etched sample reacted at 400°C for 25 hours.

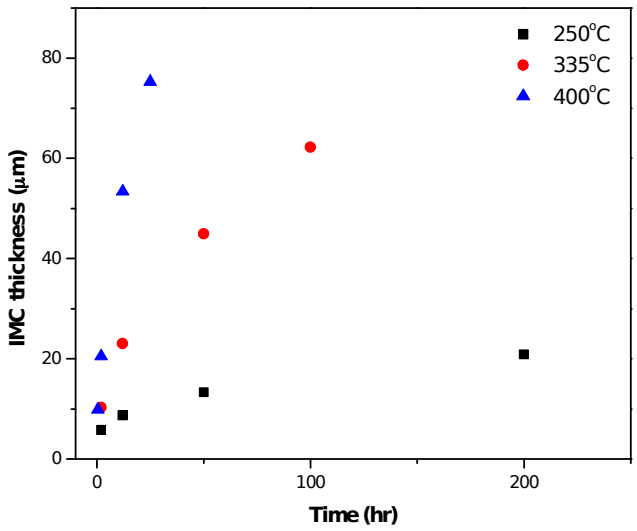

(a)

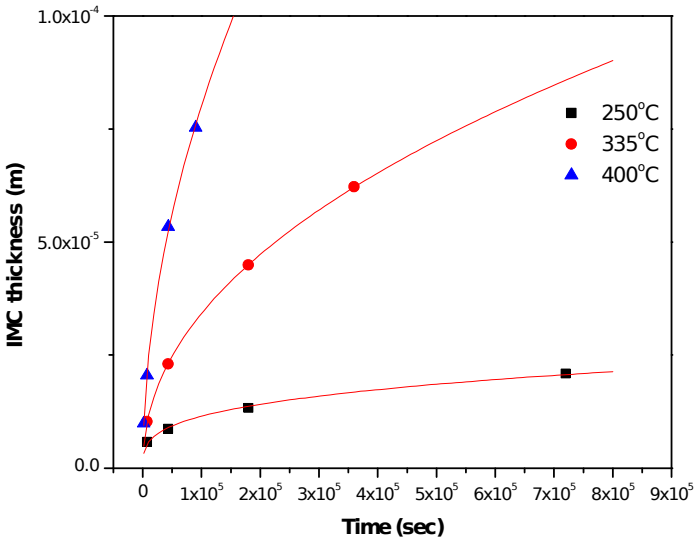

(b)

Figure 5 (a) Variation in the average thickness of the IMC with annealing time at 250°C, 335°C and 400°C and (b) The curves represent the fits of data by regression with the equation $d = kt^n$.

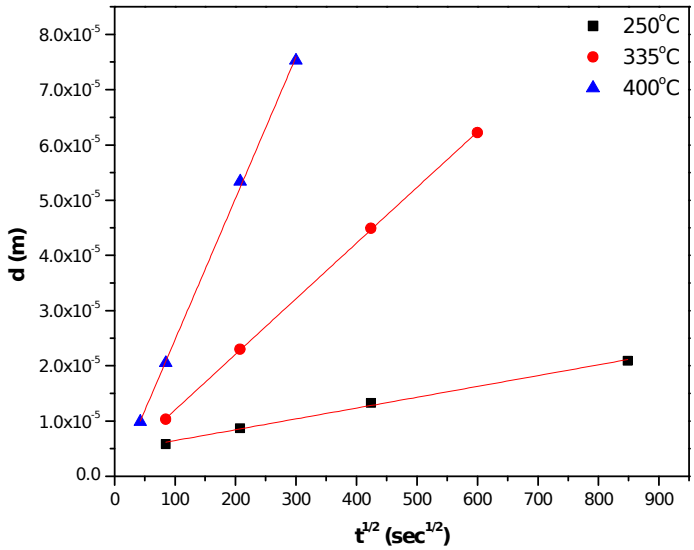

Figure 6 Variation in the average thickness of the IMC as a function of the square root of annealing time at 250°C, 335°C and 400°C. The straight lines represent fits of the data by linear regression.

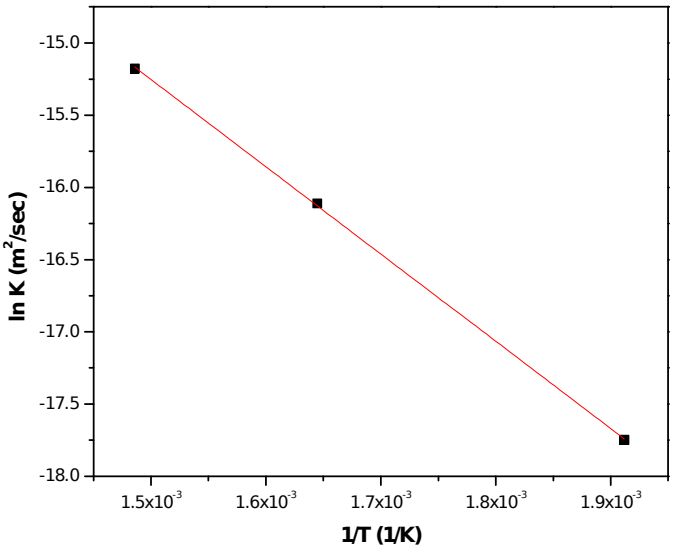

Figure 7 Arrhenius plot for evaluating the activation energy for the growth of IMC. The straight line represents a fit of the data by linear regression.

Table 1 EDX analysis of the IMC compostion at Sn/Fe interface at different annealing temperatures.

Annealing Temperature	Composition (atomic %)	
(°C)	Fe	Sn
250	32.7	67.3
335	32.5	67.5
400	32.2	67.8